

# INITIAL AND BOUNDARY VALUE APPROACHES FOR THE MULTI-TARGET TRACKING PROBLEM

L. Pirovano<sup>(1)</sup> and R. Armellin<sup>(2)</sup>

<sup>(1)</sup>*Surrey Space Centre - University of Surrey, United Kingdom, l.pirovano@surrey.ac.uk*

<sup>(2)</sup>*Surrey Space Centre - University of Surrey, United Kingdom, r.armellin@surrey.ac.uk*

## ABSTRACT

Untraced space debris are the principal threat to the functioning of operational satellites whose services have become a fundamental part of our daily life. Small debris between 1 and 10 cm are currently too small to be cataloged and are only detectable for a limited amount of time when surveying the sky. The very-short arc nature of the observations makes it very difficult to perform precise orbit determination with only one passage of the object over the observing station. For this reason the problem of data association becomes relevant: one has to find more observations of the same resident space object to precisely determine its orbit. This paper focuses on multi-target tracking, which is part of the data association problem and deals with the challenge of jointly estimating the number of observed targets and their states from sensor data. We propose a new method that builds on the admissible region approach and exploits differential algebra to efficiently estimate uncertainty ranges to discriminate between correlated and uncorrelated observations. The multi-target tracking problem is formulated with two different mathematical conditions: as initial-value problem and as boundary-value problem. The first one allows us to define the constraints as a six-dimensional region at a single epoch for each observation, while the second one, instead, allows us to consider the two-by-two comparison as a Lambert's problem thus constraining the position vectors at the two epochs. The efficiency and success rate of the two formulations is then evaluated.

Key words: Multi-target tracking, differential algebra, admissible region, initial value problem, boundary value problem.

## 1. INTRODUCTION

The problem of determining the state of resident space objects (RSOs) is fundamental to maintain a collision-free environment in space, predict space events and perform activities. Due to the development of new observing technologies and the ever-growing number of RSOs, the number of observations available is increasing by the day.

This calls for more efficient methods able to deal with the amount of data produced. Furthermore, when surveying the sky, the short-arc nature of the observations does not allow for precise orbit determination during a single passage of the object over an observing station: more short-arcs pertaining to the same object are necessary to determine a track. This process is called data association. Within the data association problem, the multi-target tracking (MTT) problem has gained relevance. It refers to the problem of jointly estimating the number of targets and their states from sensor data. It is especially necessary for too-short observations where current initial orbit determination (IOD) methods fail, as highlighted in [9]. We propose a new method that builds on the admissible region (AR) approach and exploits differential algebra (DA) to efficiently estimate uncertainty ranges to discriminate between correlated and uncorrelated observations. The uncertainty is defined in six dimensions thus determining a region of *Admissible States*, called admissible states region (ASR). This region is subsequently pruned when a new observation is acquired to remove the states that do not match with new observations. The pruning is enabled by the automatic domain splitting (ADS) tool, which estimates and controls the truncation error of the polynomial expansions in DA: whenever the tolerance is not respected, the domain over which the expansion is determined is halved and two new expansions determined. This tool is exploited in this work during propagation. Every time a new observation is available, the ASR available is compared against the newly created ASR. If there exists at least a sub-domain in common to the two ASRs, a temporary track is formed, where the new ASR is the intersection of the two. Whenever the intersection is the empty set, the track is discarded. The MTT problem is here formulated with two different mathematical conditions: as initial-value problem (IVP) and as boundary-value problem (BVP). The first one allows us to determine the ASR as a six dimensional region at a single epoch for each observation. The region is then propagated each time a new observation is available to look for intersections. The second one, instead, allows us to consider the two-by-two comparison as a Lambert's problem thus determining the ASR as a composition of position vectors from the two epochs. The intersection of the ASR is then found by comparing the velocity vectors at the two epochs and the outcome of the Lambert's

algorithm. Section 2 contains all the mathematical tools necessary to build the algorithm: Section 2.1 gives an overview on DA, Section 2.2 describes linear regression, while Section 2.3 introduces the AR. Section 3 defines the algorithm for the IVP setup while Section 4 that for the BVP approach. Results are displayed in terms of associations found and computing time in Section 5, while conclusions and future works are discussed in Section 6.

## 2. MATHEMATICAL TOOLS

### 2.1. Differential Algebra

This work makes use of DA, a computing technique that uses truncated power series (TPS) instead of numbers to represent variables [1]. By substituting the classical implementation of real algebra with the implementation of a new algebra of Taylor polynomials, any deterministic function  $f$  of  $v$  variables that is  $\mathcal{C}^{k+1}$  in the domain of interest  $[-1, 1]^v$  is expanded into its Taylor polynomial up to an arbitrary order  $k$  with limited computational effort [3, 4]. The notation for this is:  $f \approx \mathcal{T}_f^{(k)}$ . Similarly to algorithms for floating point arithmetic, various algorithms were introduced in DA, including methods to perform composition of functions, to invert them, to solve non-linear systems explicitly, and to treat common elementary functions [2]. Ultimately, this technique allows for the definition of analytical solutions of complicated systems of equations which normally require numerical techniques to be solved.

### 2.2. Linear Regression

A list of observed angles in consecutive epochs for a single object is called tracklet. Tracklets usually contain five or more observations, each observation being made of a right ascension  $\alpha$ , a declination  $\delta$ , a precision  $\sigma$  and a time of observation  $t$ . To account for sensor level errors, the precision of the observation can be modeled as white noise and thus be considered as a Gaussian random variable with zero mean and  $\sigma$  standard deviation [10]:

$$\mathbf{Y} \sim \mathcal{N}(\mathbf{y}, \Sigma). \quad (1)$$

where, for the case of optical observations analyzed in this paper, the observed values  $\mathbf{y}$  are the right ascension  $\alpha$  and the declination  $\delta$ . When tracklets are too short, information about curvature is very scarce and the tracklet can be linearly approximated [11]. This happens especially in the case of Geostationary Earth Orbits (GEOs), where the apparent null motion with respect to the observatory enhances the problem of gaining information about the curvature of the orbit. In this case, the distribution of the right ascension and declination can be linearly regressed with respect to time, following the well known

linear regression equation  $\hat{\mathbf{Y}} = \hat{\beta}_0 + \hat{\beta}_1 \mathbf{X}$ :

$$\begin{bmatrix} \hat{\alpha} \\ \hat{\delta} \end{bmatrix} = \begin{bmatrix} \hat{\alpha}_0 \\ \hat{\delta}_0 \end{bmatrix} + \begin{bmatrix} \hat{\alpha} \\ \hat{\delta} \end{bmatrix} t \quad (2)$$

In case of different precision within the same tracklet, weights can be constructed as the inverse of the square precision ( $w = \sigma^{-2}$ ). The regression can be conveniently performed at the central time of observation (C) so that the resulting slope and intercept are uncorrelated. The four dimensional vector containing the estimated values  $(\hat{\alpha}_C, \hat{\delta}_C, \hat{\alpha}, \hat{\delta})$  is known as *Attributable*. The quantity

$$T = \frac{\hat{\beta} - \beta}{s_{\hat{\beta}}} \sim t_{N-2} \quad (3)$$

is known to be distributed as a Student's T [5], where  $\hat{\beta}$  stands for any of the 4 estimated coefficients that constitute the Attributable,  $N$  is the number of fitted parameters and  $s_{\hat{\beta}}$  is standard estimate (SE) of the coefficient  $\hat{\beta}$ . The covariance of the Attributable is a diagonal matrix whose elements can be written as a function of  $N$ , the root mean square error (RMSE) of the regression  $s_{\hat{\mathbf{Y}}}$  and the tracklet length  $\Delta t$

$$\Sigma_{(\hat{\beta}_0, \hat{\beta}_1)} = s_{\hat{\mathbf{Y}}} \begin{pmatrix} \frac{1}{N} & 0 \\ 0 & \frac{12}{N(N+1)(N-1)\Delta t^2} \end{pmatrix} \quad (4)$$

where  $(\hat{\beta}_0, \hat{\beta}_1) = \{(\hat{\alpha}_C, \hat{\alpha}), (\hat{\delta}_C, \hat{\delta})\}$ . This result is obtained by considering the covariance definition

$$\begin{aligned} \Sigma_{(\hat{\beta}_0, \hat{\beta}_1)} &= s_{\hat{\mathbf{Y}}}^2 (H^T H)^{-1} = \\ &= \frac{s_{\hat{\mathbf{Y}}}^2}{N \sum_i x_i^2 - (\sum_i x_i)^2} \begin{pmatrix} \sum_i x_i^2 & -\sum_i x_i \\ -\sum_i x_i & N \end{pmatrix} \end{aligned} \quad (5)$$

where  $H_i = [1 \ t_i - t_C]$ . Remembering that we are performing the regression at the central time of observation, differently from [7] who perform it at  $t = t_0$ , the following holds:

- $\sum_i x_i = 0$  and thus  $\bar{x} = 0$ . This is exploited to obtain a diagonal matrix, thus uncorrelated coefficients.
- $\sum_i x_i^2 = \sum_{i=-\frac{N-1}{2}}^{\frac{N-1}{2}} \Delta t^2 i^2 = 2\Delta t^2 \sum_{i=1}^{\frac{N-1}{2}} i^2 = \frac{N(N+1)(N-1)\Delta t^2}{12}$

Confidence intervals (CI) of predicted values can be constructed through the covariance of the predicted quantity and the Student's T quantiles. Given a predicted value  $\hat{\beta}$ :

$$\text{C.I.: } \left[ \hat{\beta} \pm t_{1-\frac{\alpha}{2}, n-2} \cdot \sqrt{\text{Cov}(\hat{\beta})} \right] \quad (6)$$

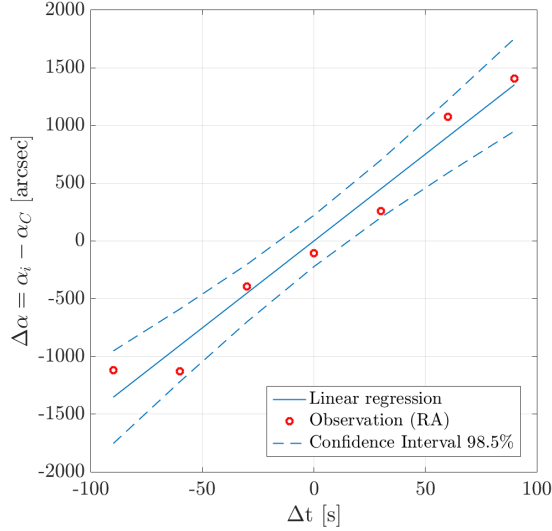


Figure 1. Regression for the right ascension  $\alpha$  centered at the central time of observation. Values are amplified by a factor 1000 for clarity purpose. The black dot and arrow represent respectively the predicted value and its IC for the central time of observation.

where  $\alpha_L$  defines the confidence level and  $\hat{\beta}$  stands for any of the attributable components, with their respective covariance matrices. Fig. 1 summarizes the regression showing the observations (dots), the mean prediction (solid line) and the CI (dashed lines).

### 2.3. Admissible Region

The Admissible Region (AR) is an approach introduced by [8] to handle too-short arcs where classical methods for IOD fail. The method gathers all the information available within the attributable and determines the set of ranges and range-rates achievable depending on physical constraints: by setting a maximum eccentricity and a minimum and maximum semi-major axis for the orbit, the 2D region in the  $(\rho, \dot{\rho})$ -plane that satisfies the constraints can be determined. For each point in the plane, then, the state of the object is defined. Fig. 2 shows the AR for a too-short arc simulated from object 36830<sup>1</sup>. The constraints are found by exploiting the equations for energy and angular momentum [6]. The constraints used to build Fig. 2 are:  $a_{min} = 20,000$  km,  $a_{max} = 60,000$  km,  $e_{max} = 0.75$ , where the values are respectively minimum semi-major axis, maximum semi-major axis and maximum eccentricity. These constraints comprise both GEOs and geostationary transfer orbits (GTOs), which can both be observed when looking at the geostationary area. The method, however, does not consider any uncertainty in the observations.

<sup>1</sup>The object numbers used throughout the paper refer to the NORAD ID in <https://www.space-track.org/>

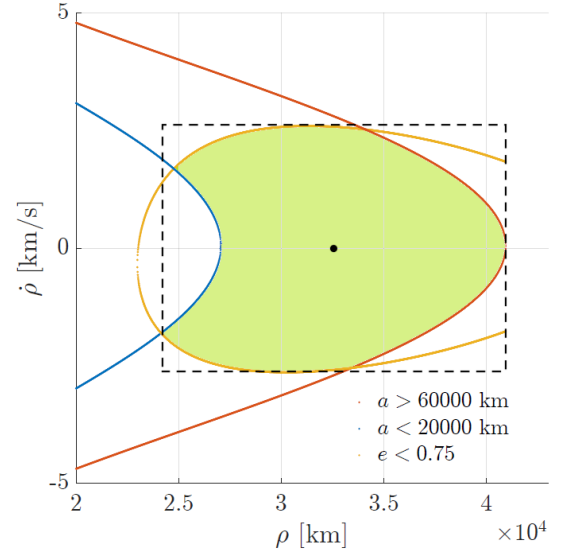


Figure 2. Admissible region for a too short arc of observed object 36830, enclosed by a dashed rectangle. The black dot is the center of the rectangle.

### 3. IVP SETUP

When setting the resolution for the MTT problem as an IVP, one defines the conditions at  $t = t_0$  and then propagates forward. Firstly, the ASR at  $t_0$  is defined. To do so, we consider the state in polar coordinates

$$\mathbf{X} = [\rho, \dot{\rho}, \alpha, \dot{\alpha}, \delta, \dot{\delta}]^T \quad (7)$$

to exploit both the knowledge on the AR  $(\rho, \dot{\rho})$  and on the attributable  $(\alpha, \dot{\alpha}, \delta, \dot{\delta})$ . The state is initialized as DA variable to include all possible combinations of the uncertain state components. The point solution and uncertainty for range and range-rate are highlighted respectively with the black dot and dashed box in Fig. 2, while the uncertain attributable is defined as the predicted value at central time of observation and its IC.

$$\mathbf{X}_0 = \begin{bmatrix} \rho_0 \\ \dot{\rho}_0 \\ \hat{\alpha}_0 \\ \hat{\delta}_0 \\ \hat{\dot{\alpha}}_0 \\ \hat{\dot{\delta}}_0 \end{bmatrix} + \frac{1}{2} \begin{bmatrix} \Delta\rho_{AR,0} \\ \Delta\dot{\rho}_{AR,0} \\ IC_{\alpha_L, \alpha_0} \\ IC_{\alpha_L, \dot{\alpha}_0} \\ IC_{\alpha_L, \delta_0} \\ IC_{\alpha_L, \dot{\delta}_0} \end{bmatrix}^T \begin{bmatrix} \delta x_1 \\ \delta x_2 \\ \delta x_3 \\ \delta x_4 \\ \delta x_5 \\ \delta x_6 \end{bmatrix} \quad (8)$$

$\delta x \in [-1, 1]$  is the achievable variation. The propagated state is thus a function of the initial six-dimensional state:

$$\mathbf{X}_t = \mathcal{T}_{\mathbf{X}_t}(\mathbf{X}_0) \quad (9)$$

Since the initial state is propagated through the use of ADS to keep the map accuracy controlled, the final map is actually a list of polynomials in the form of Eq. (9):

$$\mathbf{X}_t = \bigcup_i \mathcal{T}_{i, \mathbf{X}_t}(\mathbf{X}_0) \quad (10)$$

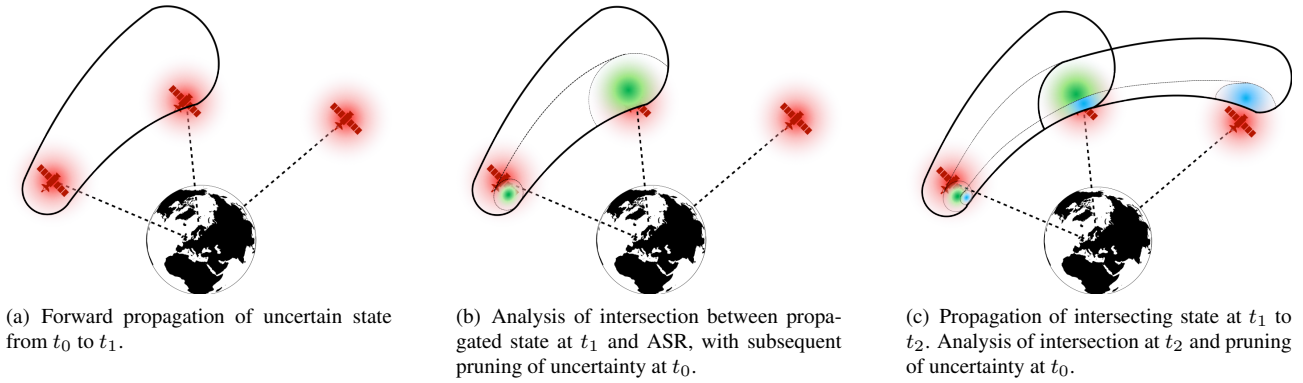


Figure 3. IVP setup for three observations.

A sketch of the uncertainty propagation is shown in Fig. 3(a). At each  $t_{obs}$ , an AR and linear regression can be performed, thus obtaining the ASR  $\mathbf{X}_{t_{obs}}$  in the form of Eq. (8) and shown in Fig. 3 as red regions. The propagated state can thus be compared with the newly obtained data by means of range intersection: if there exists an intersection between the achievable values for each component of the state vector, then the two observations are temporarily coupled. Fig. 3(b) shows the intersection (green) and the portion of initial domain kept, while the remaining initial domain is discarded. This part of initial domain is then propagated forward where a new observation is available and the same procedure is completed (Fig. 3(c)). The advantage of this method is the possibility of handling as many observations as necessary and the possibility to include perturbations in the dynamics. Whenever an intersection cannot be found, the two observations are regarded as uncorrelated and the temporary track discarded. This can be seen in Fig. 4. This procedure was introduced in [9].

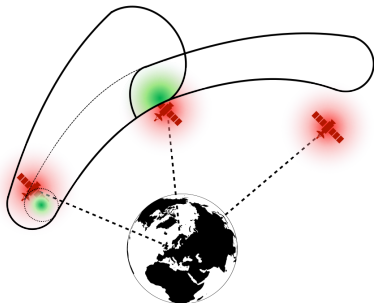


Figure 4. Example of uncorrelation for IVP setup.

#### 4. BVP SETUP

Opposed to the IVP set up, there is the BVP approach. Here the state vector is composed of the position vectors at  $t_0$  and  $t_1$ :

$$\mathbf{X}_{0,1} = [\rho_0, \alpha_0, \delta_0, \rho_1, \alpha_1, \delta_1]^T, \quad (11)$$

and conditions are set at the boundaries of the domain, that is at the two times of observations:

$$\mathbf{X}_{0,1} = \begin{bmatrix} \rho_0 \\ \hat{\alpha}_0 \\ \hat{\delta}_0 \\ \rho_1 \\ \hat{\alpha}_1 \\ \hat{\delta}_1 \end{bmatrix} + \frac{1}{2} \begin{bmatrix} \Delta\rho_{AR,0} \\ \text{IC}_{\alpha_L,\alpha_0} \\ \text{IC}_{\alpha_L,\delta_0} \\ \Delta\rho_{AR,1} \\ \text{IC}_{\alpha_L,\alpha_1} \\ \text{IC}_{\alpha_L,\delta_1} \end{bmatrix}^T \begin{bmatrix} \delta x_1 \\ \delta x_2 \\ \delta x_3 \\ \delta x_4 \\ \delta x_5 \\ \delta x_6 \end{bmatrix} \quad (12)$$

An ADS-based Lambert's solver can thus be implemented to find the list of orbits that fit these two uncertain states, namely  $L_{\{0,1\}}$  in Fig. 5(a), finding the velocities at the boundaries (Fig. 5(a)):

$$\begin{aligned} \mathbf{V}_{0,1} &= [\dot{\rho}_0, \dot{\alpha}_0, \dot{\delta}_0, \dot{\rho}_1, \dot{\alpha}_1, \dot{\delta}_1]^T \\ &= \bigcup_i \mathcal{T}_{i,\mathbf{V}_{0,1}}(\mathbf{X}_{0,1}) \end{aligned} \quad (13)$$

However,  $(\dot{\rho}, \dot{\alpha}, \dot{\delta})_{0,1}$  are already available from the attributable and AR and can thus be compared against the newly obtained map in Eq. (13). Again, only the portions of the initial domain that produce a 6D intersection are retained (Fig. 5(b)). When a third observation becomes available, one has to set new boundary conditions, analyzing the list of fitting orbits through  $t_1$  and  $t_2$  (Fig. 5(c)). Here a further check is made to make sure that the pruned domain obtained from  $L_{\{0,1\}}$  and  $L_{\{1,2\}}$  does overlap (Fig. 5(d)). This check is a necessary condition for correlation, however not sufficient: it is indeed not ensured that the 6 found intersections happen for a specific point of the initial domain. The only way to be completely sure about the correlation is to perform compute  $L_{\{0,2\}}$  and check the intersecting domains at both times (Figs. 5(e) and 5(f)). Whenever either one of the Lambert solvers or an intersection produce an empty set, the temporary track is discarded, as sketched in Fig. 6.

#### 5. RESULTS

To test the success rate and speed of the two methods, a realistic observing scenario was simulated. The test case

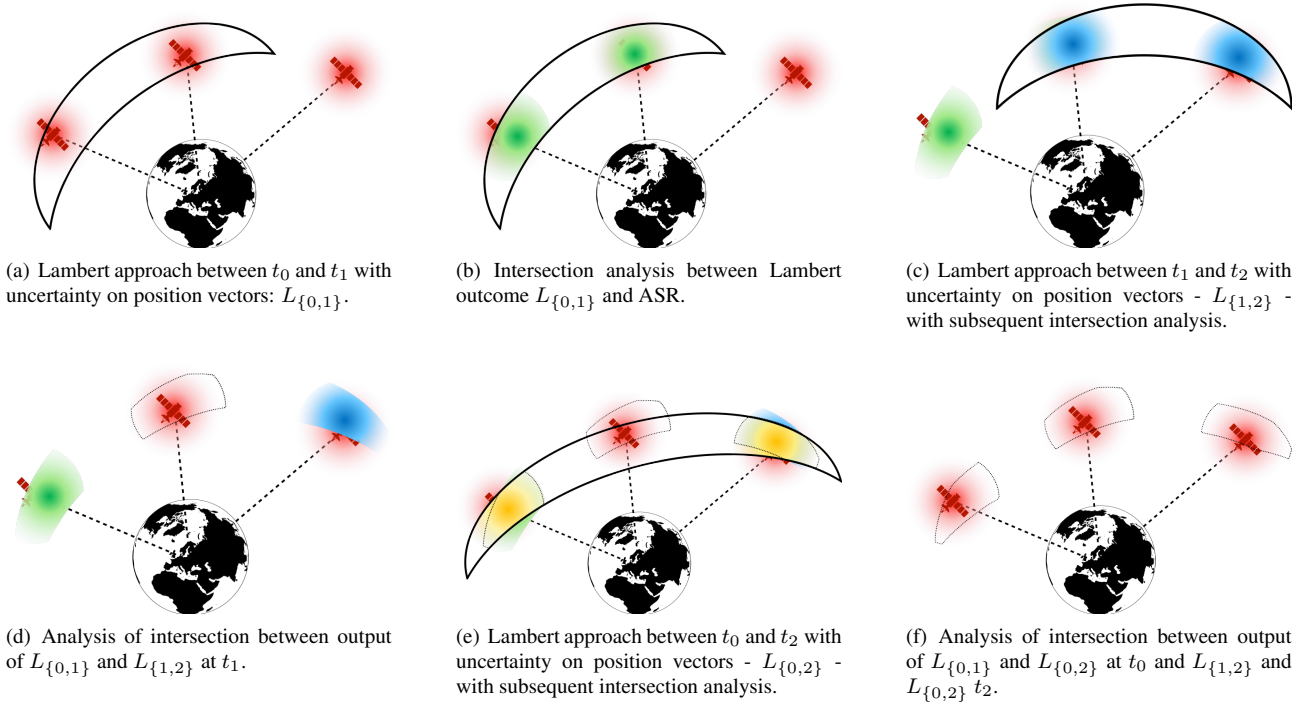


Figure 5. BVP setup for three observations.

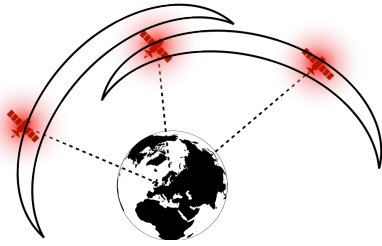


Figure 6. Example of uncorrelation for BVP setup.

follows the strategy presented in [12]: six objects in geostationary Earth orbit (GEO) were observed in the same field of view every two hours in a four hours span, with precision  $\sigma = 1$  arcsec. Here an assumption is made that every object is re-observed and the dynamics is keplerian. Fig. 7 shows the values for the right ascension and declination of the six objects observed, where object F has been created to be part of the clustered objects represented. The algorithm needs to analyze all possible couples in the first two observation slots and decide which are correlated, then go on to the third observation slot and continue the correlation process. The main difference that can be noticed straight away between the IVP and BVP methods, is the treatment of a fourth or more observation: while the IVP can handle as many consecutive observations as needed, the BVP setup needs to re-set the boundary conditions and make increasing checks on each couple, thus slowing down the process. Nevertheless, it is possible to firstly assess their performance on the first three observing slots and then decide which strategy to adopt later.

Table 9(a) shows the results in terms of identified tracks and computing time, obtained with a MacBook Pro, 2.6 GHz, Intel Core i5. The tolerance for the ADS was set to 1 km for range, 1 m/s for range rate,  $10^{-6}$  arcsec for angles and  $10^{-10}$  arcsec/s for angular rates. The CIs were obtained with confidence level  $\alpha_L = 1\%$ . Both methods were able to identify all tracklets. However, the IVP algorithm created many more false tracks than the BVP, where the only false correlation can be discarded by post-processing the correlations found. The false tracks were all created starting from the clustered objects, where distinguishing the objects is more difficult, as expected. A great difference is found in the computing time, where the BVP approach outperformed the IVP by one order of magnitude. The results clearly show that the BVP method was able to spot the correct correlations in less

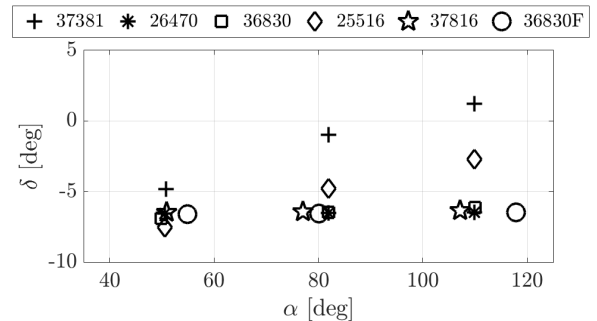


Figure 7. Right ascension and declination of six objects observed three times over a four hours time.

Table 1. IVP and BVP results for association and computing time.

	True Positive	False Positive	False Negative	Computing Time
IVP	6	5	0	414.7 s
BVP	6	1	0	45.0 s

time. On the other hand, however, it has trouble handling more than three observations: indeed, the Lambert routine has to be performed  $N - 1$  times each time an  $N$  observation is available, thus reducing the efficiency of the tool. Looking at Fig. 8, one can clearly notice that the biggest effort for the IVP approach is spent on the first correlation (Fig. 9(b)), while the second correlation involves a much smaller domain. This suggests that an hybrid approach may be the best solution: adopt the BVP approach for the first two or three observations, and then associate new observation with forward propagation as in the IVP approach. Indeed, Fig. 9 shows that the BVP approach created much less domains during the first two correlations, was faster and had a much higher success rate for correlations. Increasing the confidence level  $\alpha_L$ , it was noted that the computation time decreased but some false negatives were also found, while decreasing it boosted the number of false positives and computing time, as expected.

## 6. CONCLUSION AND FUTURE WORK

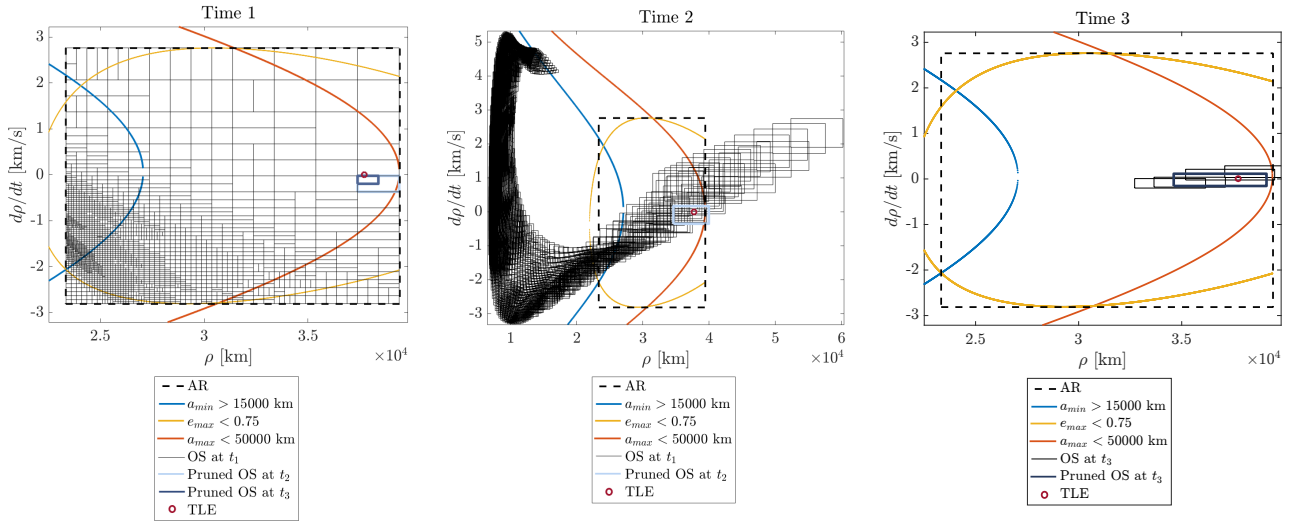
This paper analysed a novel approach to tackle the MTT problem by exploiting a high-order method that enables a semi-analytical description of the uncertainty region associated to an optical observation. The AR approach and linear regression were used to define the physical boundaries of the variables, given that current IOD methods fail when the observed arc is too short.

Two different approaches were described in this papers. With the IVP approach, conditions were set at the initial time of observation. This defined the ASR, which was then propagated forward and checked against the following ASRs. Whenever the intersection produced an empty set, the temporary track was discarded. With the BVP approach, conditions were set at the boundary of the working environment, that was at the two times of observations considered. The ASR thus consisted of the two position vectors and the full state was obtained through a Lambert routine. For each new observation, the conditions were changed and a new Lambert routine performed. Structure-wise, the IVP approach seemed more suitable to deal with any number of new observations, since the initial conditions never changed and only forward propagation was performed. Indeed, the Lambert routine had to be performed  $N - 1$  times each time an  $N$  observation is available. Nevertheless, results showed that the BVP was one order of magnitude faster when looking for correlation for six GEO objects observed three times and only created one false correlation (easily discarded by post-processing the correlations found). The reason why less time was needed was that uncer-

tainty propagated much faster in the IVP approach, as shown in the projection of the ASR over the AR. This suggested the possibility of implementing an hybrid approach to take advantage of all strengths of the two methods: on one side the efficiency of the BVP to start the correlation process, on the other the possibility of correlating more than three observations with only one forward propagation with the IVP approach. The implementation of an hybrid approach is thus the next step of this study.

## REFERENCES

1. Armellin, R. & Di Lizia, P. *Probabilistic initial orbit determination* in 26th AAS/AIAA Space Flight Mechanics Meeting (Feb. 2016), 1–17.
2. Berz, M. *Differential Algebraic Techniques, Entry in Handbook of Accelerator Physics and Engineering* (World Scientific, New York, 1999).
3. Berz, M. The method of power series tracking for the mathematical description of beam dynamics. *Nuclear Instruments and Methods A258* (1987).
4. Berz, M. *The new method of TPSA algebra for the description of beam dynamics to high orders* Los Alamos National Laboratory (1986).
5. Casella, G. & Berger, R. *Statistical Inference* (Duxbury Resource Center, June 2001).
6. DeMars, K. J. & Jah, M. K. Probabilistic Initial Orbit Determination Using Gaussian Mixture Models. *Journal of Guidance, Control, and Dynamics* **36**, 1324–1335 (2013).
7. Fujimoto, K. & Alfriend, K. T. Optical Short-Arc Association Hypothesis Gating via Angle-Rate Information. *Journal of guidance, Control, and Dynamics* **38**, 1602–1613 (2015).
8. Milani, A., Gronchi, G., de' Michieli Vitturi, M. & Knezevic, Z. Orbit determination with very short arcs. I admissible regions. *Celestial Mechanics and Dynamical Astronomy* **90**, 59–87. ISSN: 09232958 (2004).
9. Pirovano, L., Santeramo, D. A., Armellin, R., Di Lizia, P. & Wittig, A. *Probabilistic data association based on intersection of Orbit Sets* in 19th AMOS Conference, September 11-14, 2018, Maui, USA (Sept. 2018).
10. Poore, A. B. *et al. Covariance and Uncertainty Realism in Space Surveillance and Tracking* tech. rep. (Numerica Corporation Fort Collins United States, 2016).
11. Siminski, J. *Object correlation and orbit determination for geostationary satellites using optical measurements* PhD thesis (Bundeswehr University Munich, Oct. 2016).
12. Zittersteijn, M., Vananti, A., Schildknecht, T. & Martinot, V. *A Genetic Algorithm to associate optical measurements and estimate orbits of geocentric objects* in European Conference for Aerospace Science (2015).

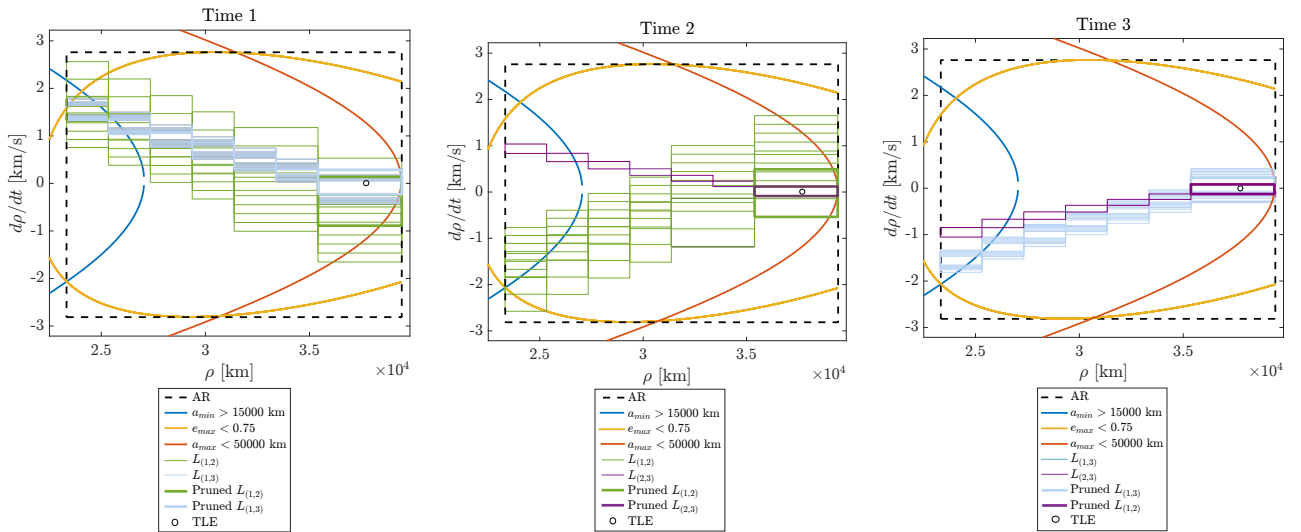


(a) Admissible region at  $t_1$ . Splitting is performed during propagation to  $t_2$ . Light-blue box is the intersecting uncertainty between  $t_1$  and  $t_2$ . Blue box is the intersecting uncertainty among  $t_1$ ,  $t_2$  and  $t_3$ .

(b) Propagated uncertainty from  $t_1$  to  $t_2$  with selection of intersecting uncertainty.

(c) Propagation of intersecting uncertainty from  $t_2$  to  $t_3$  and selection of further intersection.

Figure 8. IVP approach: sequential pruning of Admissible Region for observed object 36830. All pruned boxes contain true solution.



(a) Projection of Lambert outcomes  $L_{\{1,2\}}$  and  $L_{\{1,3\}}$  on Admissible Region at  $t_1$ . Intersection between the two outcomes is presented in bold.

(b) Projection of Lambert outcomes  $L_{\{1,2\}}$  and  $L_{\{2,3\}}$  on Admissible Region at  $t_2$ . Intersection between the two outcomes is presented in bold.

(c) Projection of Lambert outcomes  $L_{\{2,3\}}$  and  $L_{\{1,3\}}$  on Admissible Region at  $t_3$ . Intersection between the two outcomes is presented in bold.

Figure 9. BVP results at three times of observation for observed object 26470. All pruned intersections contain the true solution.